JOURNAL OF APPLIED ELECTROCHEMISTRY **28** (1998) 1419–1428

Steady-state mass transfer between two opposite discs and a liquid in radial divergent flow

E. BEZERRA CAVALCANTI*, F. COEURET‡

CNRS–UMR no. 6607 Nantes, Laboratoire de Thermocinétique, implantation Ecole Louis de Broglie, Campus de Ker Lann, 35170 Bruz, France

Received 10 December 1997; accepted in revised form 26 May 1998

The paper deals with global and local mass transfer between a liquid and two opposite fixed discs. The liquid is introduced through a central hole in one of the discs and flows radially. The mass transfer coefficients, measured by the electrochemical method, are empirically correlated. The correlations are compared with corresponding empirical correlations from the literature. Local measurements using microelectrodes allowed to determine the evolution of the local mass transfer coefficients over each disc as a function of the geometrical parameters, particularly the gap between the discs.

Keywords: *empirical correlation*, *mass transfer*, *radial flow*, *transfer coefficients*

List of symbols

C	concentration (mol m^{-3})
D	molecular diffusion coefficient of ferricyanide ions (m^2 s^{-1})
$f(z)$	dimensionless function representing the velocity profile
h	half distance between the discs, or between the plates (m)
I_L	limiting diffusion current (A)
$\bar{k}_d$	average mass transfer coefficient (m s^{-1})
$k_d(r)$	local mass transfer coefficient (m s^{-1})
$(\bar{k}_d)_I$	average mass transfer coefficient at disc D_I (m s^{-1})
$(\bar{k}_d)_S$	average mass transfer coefficient at disc D_S (m s^{-1})
L	length of a plate in a rectangular channel flow (m)
Q_v	volumetric flow rate (m^3 s^{-1})
r	radial coordinate (m)
R_1	radius of the central hole in disc D_I (m)
R'_1	radius of the entrance region at disc D_I (m)
R_2	external radius of the discs (m)
Re	Reynolds number ($=Q_v/(2hv)$)
Re'	Reynolds number in Equation 8 ($=\bar{v}2h/v$)
Re_m	channel Reynolds number at r ($=Q_v/(4\pi hv)$)
Sc	Schmidt number ($=v/D$)
$\overline{Sh}$	Sherwood number based on $2h$ ($=\bar{k}_d\ 2h/D$)
$\bar{v}$	mean velocity (m s^{-1})
X	reduced variable, given by Equation 2
X_2	overall reduced variable, given by Equation 6

Greek symbols

v	kinematic viscosity (m^2 s^{-1})
ρ	density (kg m^{-3})

Subscripts

I	lower disc
S	upper disc
int.	from spatial integration of the distribution
meas.	average value from the total current

1. Introduction

Radial flow between stationary discs has been studied by different authors [1–8]. The fluid is generally introduced axially through one disc and flows radially between the discs; this type of flow is divergent. In industrial electrochemistry, divergent radial flow between discs is applied in the 'pump cell' proposed for electroorganic applications [9, 10]. In such a cell, the flow is normally generated by the rotation of one disc, but forced flow without rotation has also been considered [11, 12]. Studies related to hydrodynamic and heat transfer aspects in such configurations have also been made [13–18].

An experimental study of solid to liquid mass transfer in forced-flow systems consisting of rotating or fixed discs placed between annular, axially set discs in a cylindrical container, was undertaken [19]. Radial flow is successively divergent and convergent between pairs of discs. The program has been initiated by the study of mass transfer to two parallel discs, one rotating, the other stationary, located in a closed cylinder [20].

The present work deals with global and local mass transfer to the opposite discs in the presence of radial

* Univ. Federal da Paraiba (C.C.T./D.E.Q), Av. Aprigio Veloso, 882, Bodocongó, Campina Grande, 58100-Pb, Brazil.
‡ Author to whom correspondence should be addressed. E-mail: coeuret@isitem.univ-nantes.fr

divergent liquid flow. There is a similarity between this work and the study of mass transfer between a solid surface and a submerged liquid jet [21, 22].

2. Hydrodynamics and mass transfer in radial flow between discs

The hydrodynamics of the radial flow between two discs has been theoretically and experimentally studied [1–8, 23]. A characteristic of such a flow is that the mean velocity decreases with the radial coordinate. The case where the flow is laminar at the centre, and remaining laminar with r increasing, has been treated theoretically [2]. Flow turbulent at small values of r, may become laminar due to reverse transition at a critical coordinate $r = r_c$ [2, 15, 16]. Important contributions from two research groups are summarized below.

2.1. *Results of Kreith*

Kreith [15, 16] made theoretical and experimental heat and mass transfer studies.

2.1.1. Laminar flow. Kreith's results for heat transfer in symmetrical laminar flow can be adapted to wall-to-liquid mass transfer in the same type of flow, thus leading to the following differential equation:

$$\frac{\partial^2 C}{\partial z^2} = Re_m\, Sc\, f(z)\, \frac{1}{r}\frac{\partial C}{\partial r} \tag{1}$$

where

$$Re_m = \frac{\frac{Q_v}{4\pi r h} r}{\nu} = \frac{Q_v}{4\pi h \nu}$$

is the channel Reynolds number. Equation 1 neglects radial diffusional transport with respect to transversal diffusional transport.

Equation 1 contains the product of the dimensionless numbers Re_m and Sc. Its dimensional homogeneity is satisfied if the dimensionless ratio $2h^2/(r^2 - R_1^2)$ is associated to Re_m and Sc via a dimensionless product:

$$X = Re_m\, Sc \frac{2h^2}{r^2 - R_1^2} \tag{2}$$

where the reduced variable X was introduced by Kreith as a key variable in the development made for creeping flow considerations [16].

Kreith's theoretical solutions can be expressed in terms of radial distributions of the local mass transfer coefficients, $k_d(r)$, as follows:

(i) parabolic velocity profile:

$$k_d(r) = \frac{D}{2h}\sum_{n=0}^{\infty} 8.36\left(4n + \frac{5}{3}\right)^{-1/3} \times \exp\left[-\frac{2}{3}\left(4n + \frac{5}{3}\right)^2 \frac{1}{X}\right] \tag{3}$$

(ii) uniform velocity profile:

$$k_d(r) = \frac{D}{h}\sum_{n=0}^{\infty} 2\, \exp\left\{-\left((2n+1)\frac{\pi}{2}\right)^2 \frac{1}{X}\right\} \tag{4}$$

Spatial integration of Equations 3 and 4 between $r = R_1$ and $r = R_2$ yields the mean mass transfer coefficient $\bar{k}_d$ and the Sherwood number, $\overline{Sh} = \bar{k}_d(2h)/D$, as a function of the overall reduced variable:

$$X_2 = \frac{2Re_m\, Sc\, h^2}{R_2^2 - R_1^2} \tag{5}$$

These two theoretical solutions, tested experimentally by Kreith for both mass and heat transfer, tend to:

$$\overline{Sh} = 2X_2 = 2\left\{\frac{2\, Re_m\, Sc\, h^2}{R_2^2 - R_1^2}\right\} \tag{6}$$

when X_2 tends to zero. This limiting solution was verified experimentally by Kreith [15] for heat transfer in air, and using Thomas' data [17] for water. Equation 6 applies for $X_2 \le 0.6$. Beyond this value, and if the flow is laminar, the data seem to agree better with the solution corresponding to a parabolic velocity profile.

No physical meaning of X_2 was given by Kreith. This parameter can be expressed as follows:

$$X_2 = \frac{h^2}{D\bar{t}_s} \tag{7}$$

where $\bar{t}_s$ is the mean residence time in the cell, and Equation 7 allows Equation 6 to be reduced to $\bar{k}_d = h/\bar{t}_s$. Note that Equation 6 shows a variation of $\overline{Sh}$ with Sc, and not with $Sc^{1/3}$ as for convective mass transport through laminar boundary layers.

Equation 6 can be compared with the theoretical solution corresponding to wall-to-liquid mass transfer in laminar flow between two wide parallel flat plates of length L and separation $2h$. For fully developed boundary layer flow, the integration of a differential equation analogous to Equation 1 leads to the well known Leveque equation [25]:

$$\overline{Sh} = 1.85\,(Re'\ Sc\ 2h/L)^{1/3} \tag{8}$$

where Re' is a channel Reynolds number. However, when the diffusional mass transport takes place with a uniform velocity profile, the solution of the problem becomes [25]:

$$\overline{Sh} = \frac{2}{\pi^{1/2}}(Re'\ Sc\ 2h/L)^{1/2} \tag{9}$$

Note the similarity between X_2 and the reduced variable $Re' \times Sc \times 2h/L$, and the difference between the numerical values of its exponent in Equations 8 and 9.

2.1.2. Turbulent flow. Using experimental data of naphtalene dissolution in air ($Sc = 2.4$), Kreith [15] obtained, for a turbulent flow between the discs:

$$\overline{Sh} = 0.565\left\{\frac{2Re_m\, Sc\, h^2}{R_2^2 - R_1^2}\right\}^{0.8} = X_2^{0.8} \tag{10}$$

in which R_1 is the radius of the circular surface delimited around the centre of the disc receiving the entering flow. Curiously, Kreith did not introduce the one third power of Sc in its empirical correlation for mass transfer, until its transposition to heat transfer via the Chilton–Colburn analogy.

2.2. *Results of Jansson et al.*

Some of Jansson's experimental work in the development of the pump cell [26, 27] may be used for comparison with the results of the present work. The radial flow shown in Fig. 1(a) and (b) is divergent and free at the periphery, while that in Fig. 1(c) is successively divergent and convergent in a closed cell, that is, with a wall effect existing near the periphery of the discs. The mean mass transfer coefficient, $\bar{k}_d$, between the flowing liquid and discs A and B, respectively, or discs A′ and B′ taken as a whole (A′ and B′ were electrically connected, thus neglecting possible differences in the hydrodynamics near A′ and B′), was measured electrochemically. Radial distributions of the local mass transfer coefficient determined over surface A for several distances $2h$ show the attenuation of the entrance flow effect with decreasing $2h$. According to Ghoroghchian [26], mass transfer is stronger in divergent radial flow than in convergent radial flow.

2.3. *Graphical representation of literature data*

Table 1 contains empirical correlations found in the literature or established by the authors from published results. They express $\overline{Sh}$ as a function of X_2, and $\overline{Sh} \times Sc^{-1/3}$ as a function of X_2/Sc, for global mass transfer between a fluid in radial divergent flow and the two opposite discs [11, 26, 27]. Other results of Jansson concerned with radial convergent flow [26] or radial flow consecutively divergent and convergent [26, 27] (Fig. 1(c)), were empirically correlated by the authors. It is worth noting in Table 1 that the flow was laterally confined in the experiments of Jansson while there was no lateral confinement in the experiments of Kreith.

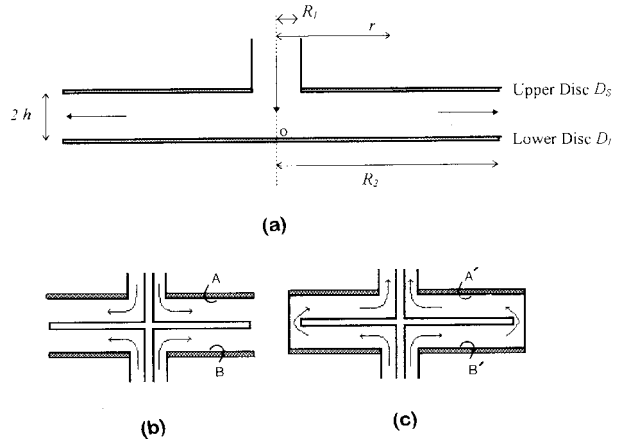

Fig. 1. Radial flows between two parallel discs. (a) Divergent (outflow) single; (b) divergent double outflow; (c) divergent/convergent (outflow/inflow).

In establishing the correlations from the data of Jansson [11, 26, 27], it was assumed that the experiments were made at 30 °C and that $Sc = 840$ (the value of the temperature was not indicated by Jansson *et al.* who used 0.1 M NaOH and only stated that Sc was about 800). Taking for the viscosity the value of the water viscosity at 30 °C and the corresponding value of $9.4 \times 10^{-10}\,m^2\,s^{-1}$ at 30 °C of the molecular diffusion coefficient of ferricyanide ions in aqueous NaOH solutions [28], a value of $Sc = 840$ is obtained.

The group of Jansson determined solid-to-liquid mass transfer coefficients by means of the electrochemical method (reduction of ferricyanide in aqueous NaOH), while Kreith measured solid to gas mass transfer coefficients using the dissolution of naphtalene in air.

Figure 2(a) compares the correlations of Table 1 in the form of the variation of $\overline{Sh}$ against X_2. The two clearly distinguishable families of curves correspond to the works of Kreith and Jansson *et al.*, respectively, that is, to $Sc = 2.4$ in the former and $Sc = 840$ in the latter. Figure 2(b) compares the empirical correlations as $\overline{Sh} \times Sc^{-1/3}$ against X_2/Sc. In Fig. 2(b) all the published results are in satisfactory agreement, indicating that $\overline{Sh}$ against X_2 is not an acceptable representation. In other words, the influence of Sc (or Pr) has to be considered as $Sc^{1/3}$ (or $Pr^{1/3}$).

3. Experimental details

The two discs of the cell were arranged as in Fig. 1(a), thus minimizing the end effects at their periphery. This cell is part of a set-up made of Altuglas, previously used in research on the impingement of liquid jets on a solid surface [21, 22]. The set-up (Fig. 3) is essentially composed of two main parts: (a) a cylindrical (internal diameter 185 mm) part, E, with a lateral exit at its top; its base supports a 60 mm diameter cylinder, F. A cylindrical piece, G, made of Altuglas (dia. 110 mm) in which a nickel disc (D_I; dia. $2R_2 = 90$ mm) is inserted, is held at its top; (b) a cylinder made of Altuglas, H, externally screwed, can be moved vertically through the cover of E. A 110 mm diameter support at the basis of this cylinder holds a nickel disc D_S (thickness 3 mm; dia. $2R_2 = 90$ mm) with active lower face and perforated at its centre (cylindrical hole diameter $2R_1 = 6$; 10 or 14 mm). The verticality of the system is ensured by a perforated disc J made of Altuglas, which can be moved by screwing it along H.

The liquid is circulated by a centrifugal pump and enters the cell at the top. The velocity profile just before the perforated disc D_S is made uniform with a cylindrical pad of stainless steel wire working as a calming section; however, owing to the reduced thickness (3 mm) of D_S, a small *vena contracta* effect is generated at the entrance. The liquid flowrate, Q_v,

Table 1. Empirical correlations from the literature for mass (heat) transfer to stationary discs in radial divergent and/or convergent flow (transfer surfaces are indicated in bold)

Authors	*Correlations and number*	*Domain of validity*	*Method*	*Cell and flow*
Jansson and Marshall [27]	$\overline{Sh} = 0.086(X_2)^{0.756} = 1.48\ Sc^{1/3}(Y_2)^{0.756}$ $[T-6]$	$3.5 \times 10^3 \le Re_m \le 2.84 \times 10^4$ $2h/R_2 = 0.025;\quad Sc = 840$	Electrochemical	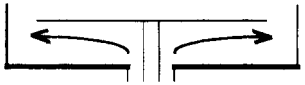
Ashworth and Jansson [11]	$\overline{Sh} = 0.11(X_2)^{0.75} = 1.82\ Sc^{1/3}(Y_2)^{0.75}$ $[T-5]$ $\overline{Sh} = 0.30(X_2)^{0.53} = 1.13\ Sc^{1/3}(Y_2)^{0.53}$ $[T-4]$	$6.3 \times 10^4 \le Re_m \le 2.6 \times 10^6$ $2h/R_2 = 0.0038;\ Sc = 840$		
Ghoroghchian *et al.* [26]	$\overline{Sh} = 0.078(X_2)^{0.77} = 1.48\ Sc^{1/3}(Y_2)^{0.77}$ $[T-7]$	$3 \times 10^3 \le Re_m \le 2.2 \times 10^4$ $2h/R_2 = 0.0253;\ Sc = 840$		
Kreith [15, 16]	$\overline{Sh} = (X_2)^{0.5} = 1.16\ Sc^{1/3}(Y_2)^{0.5}$ $[T-1]$	$650 \le Re_m \le 2.4 \times 10^4$ $0.013 \le 2h/R_2 \le 0.0625;$ $Sc = 2.4$	Dissolution	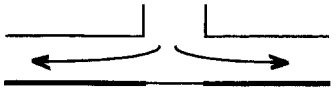
	$\overline{Sh} = 0.565(X_2)^{0.8} = 0.85\ Sc^{1/3}(Y_2)^{0.8}$ $[T-2]$	$Re_m \ge 5 \times 10^3;\ Sc = 2.4$ $0.0128 \le 2h/R_2 \le 0.0315$		
Bakke *et al.* [5]	$\overline{Sh} = 0.46(X_2)^{0.8} = 0.69\ Sc^{1/3}(Y_2)^{0.8}$ $[T-3]$	$6.2 \times 10^3 \le Re_m \le 4.8 \times 10^4$ $0.0136 \le 2h/R_2 \le 0.05$ $Sc = 2.4$		
Ghoroghchian *et al.* [26]	$\overline{Sh} = 0.18(X_2)^{0.65} = 1.52\ Sc^{1/3}(Y_2)^{0.65}$ $[T-8]$	$3.2 \times 10^3 \le Re_m \le 2 \times 10^4$ $2h/R_2 = 0.0253$ $Sc = 840$	Electrochemical	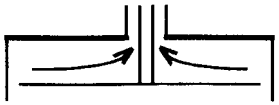
	$\overline{Sh} = 0.14(X_2)^{0.68} = 1.45\ Sc^{1/3}(Y_2)^{0.68}$ $[T-10]$	$3.2 \times 10^3 \le Re_m \le 3.2 \times 10^4$ $2h/R_2 = 0.0253$ $Sc = 840$		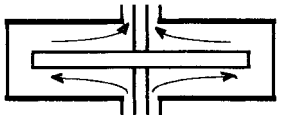
Jansson and Marshall [27]	$\overline{Sh} = 0.15(X_2)^{0.67} = 1.45\ Sc^{1/3}(Y_2)^{0.67}$ $[T-9]$	$4.1 \times 10^3 \le Re_m \le 3.2 \times 10^4$ $2h/R_2 = 0.0253$ $Sc = 840$		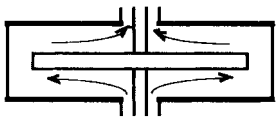
	$\overline{Sh} = 2\bar{k}_d h/D$	$X_2 = \dfrac{2Re_m\, Sc\, h^2}{R_2^2 - R_1^2}$	$Re_m = \dfrac{Q_v}{4\pi h v}$	$Y_2 = X_2/Sc$

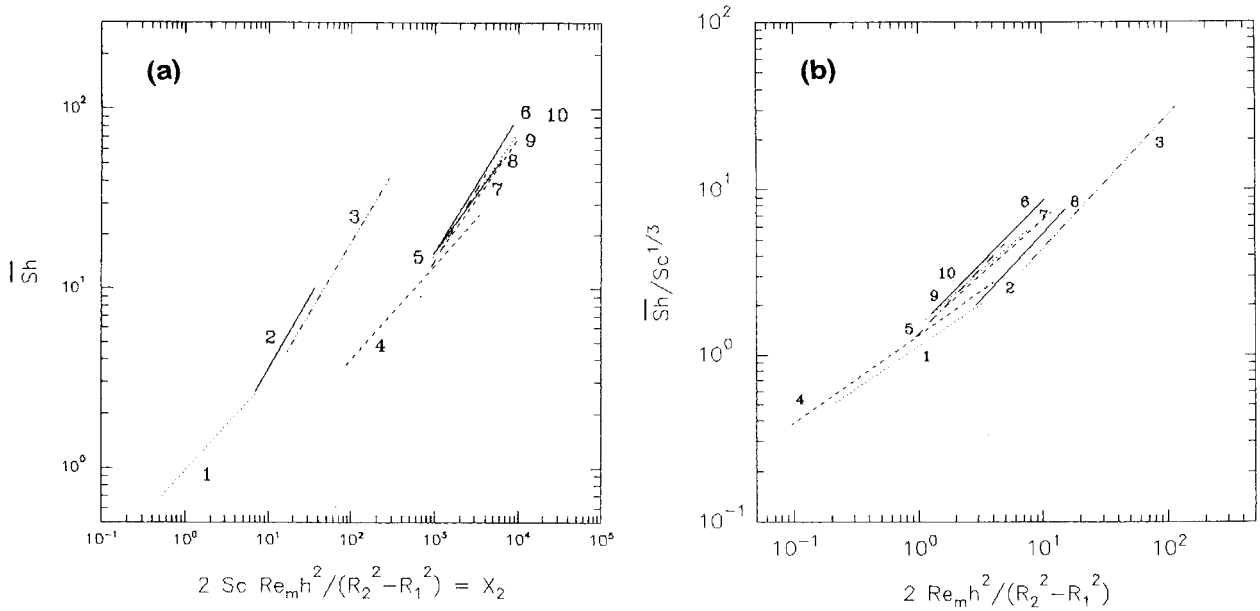

Fig. 2. Comparison of the empirical correlations in Table 1. Sources: (1, 2) Kreith [15, 16]; (3) Bakke *et al.* [5]; (4, 5) Ashworth and Jansson [11]; (6) Jansson and Marshall [27]; (7, 8) Ghoroghchian *et al.* [26]; (9) Jansson and Marshall [27]; (10) Ghoroghchian *et al.* [26].

was measured with rotameters, and it varied between 15 and 470 $dm^3 h^{-1}$.

The two nickel discs were used as electrodes in the determination of the mass transfer coefficient. In this, now classical, method [28], $Fe(CN)_6^{3-}$ ions contained in a mixture of $Fe(CN)_6^{3-}$ 0.005 M and $Fe(CN)_6^{4-}$ 0.05 M in a 0.5 M aqueous solution of NaOH are reduced. A nickel wire located approximately at the same level as D_I and D_S, but outside the channel defined by these discs, acts as a redox reference electrode. When D_S is used as the working electrode (i.e., cathode), D_I serves the counter-electrode (i.e., anode), and vice versa. The concentration of the $Fe(CN)_6^{3-}$ ions was determined amperometrically by adding cobalt salt to an ammonium media and using a rotating disc platinum electrode.

The liquid temperature was maintained at 30 °C by controlled heating of the reservoir. At this temperature, the electrolyte properties are $\nu = 0.94\times10^{-6}\,m^2 s^{-1}$, $\rho = 1050\,kg\,m^{-3}$ and $D = 8.8\times10^{-10}\,m^2 s^{-1}$; thus $Sc = \nu/D = 1070$.

Two sets of measurements were made. In the first set, global measurements dealing with entire surface areas of D_I and D_S served for the determination of the mean mass transfer coefficient $\bar{k}_d$ at each disc under given geometrical and hydrodynamical conditions. The experimental variables were R_1, h and Q_v. In the second set, local measurements were made by using 400 μm diameter nickel wires as microelectrodes inserted into 600 μm diameter cylindrical holes and held in place with Araldite. The microelectrodes were located radially in each disc (18 microelectrodes for D_I; 21 microelectrodes for D_S). The distribution, $k_d(r)$, of the local mass transfer coefficients on each disc was obtained. The measurements were restricted to $2R_1 = 6$ mm; thus the variables were only h and Q_v.

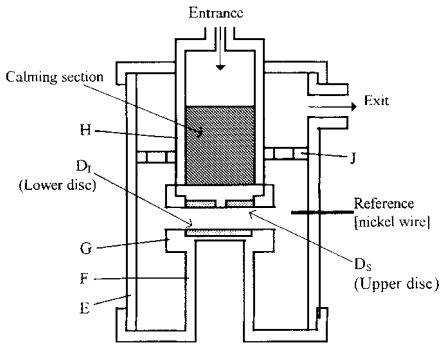

Fig. 3. Schematic view of the cell used.

The active surfaces of discs D_I and D_S, including the microelectrodes, were mechanically polished down to a roughness of 0.25 μm and were activated prior to each experiment by short contact (30 s) with a 50% aqueous solution of HCl, followed by rinsing.

The limiting diffusion current, I_L, was measured with a classical three-electrode potentiostatic circuit using a Tacussel-PRT potentiostat linked to a Tacussel Pilovit-Num pilot unit. The current–time (i.e., the current–potential) curves were registered with a Sefram-Servotrace register. When local measurements were made at a given disc, limiting currents corresponding to the whole cathodic surface and to each microelectrode were measured under the same experimental conditions, thus leading to $\bar{k}_d$ and $k_d(r)$, respectively. The numerical values of $\bar{k}_d$ and $k_d(r)$ were computed from I_L.

4. Results

4.1. *Average mass transfer*

Figure 4 presents the experimental variations of I_L as a function of Q_v, for the two discs D_I and D_S, and at different geometrical conditions. It can be observed

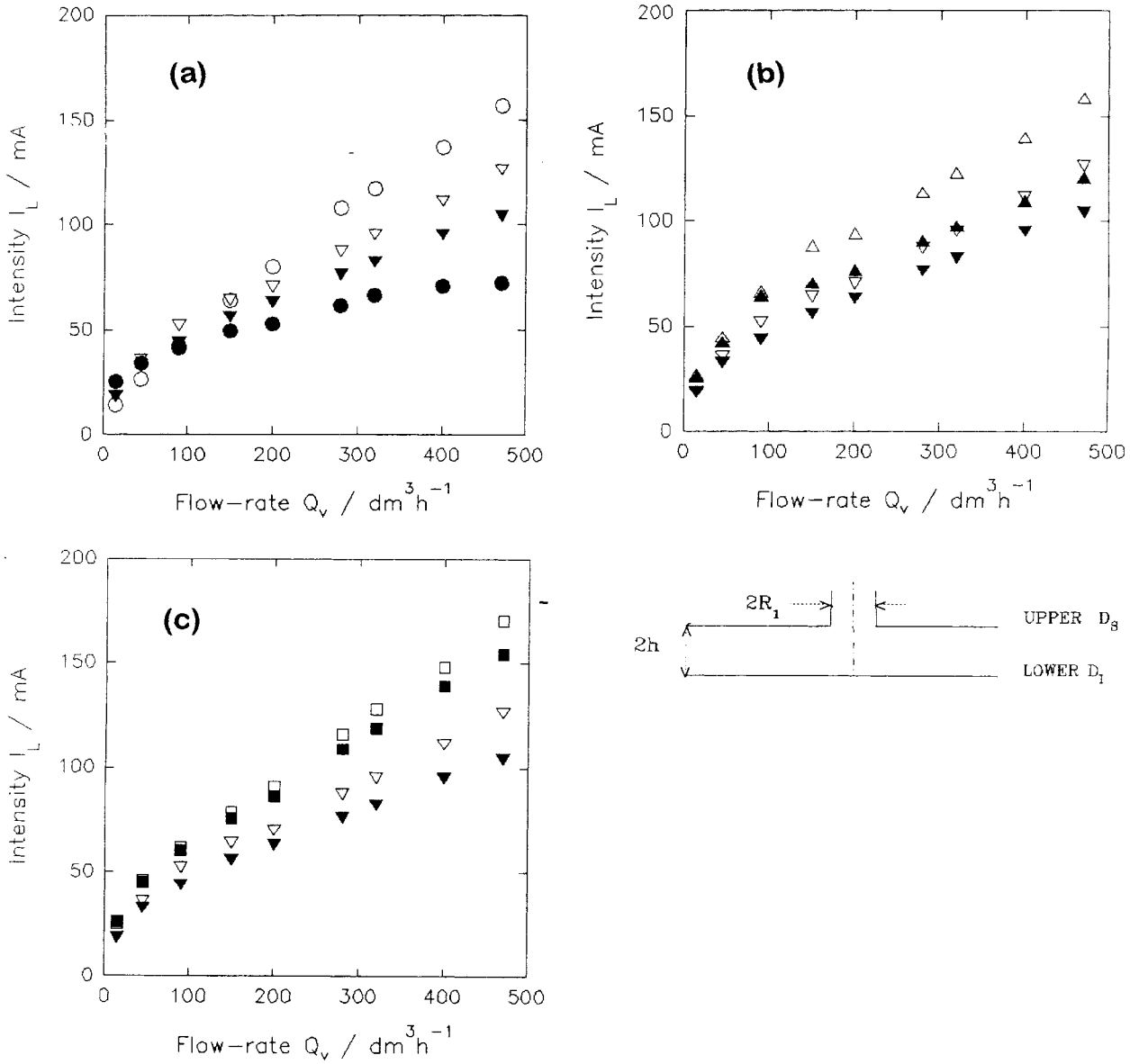

Fig. 4. Variation of the limiting current I_L to discs D_I and D_S with Q_v. (a) for $2R_1 = 14$ mm and $2h = 2$ (▽, ▼) or 6 mm (○, ●); (b) for $2R_1 = 14$ mm and $2h = 0.76$ (△, ▲) or 2 mm (▽, ▼); (c) for $2h = 2$ mm and $2R_1 = 10$ (□, ■) or 14 mm (▽, ▼). Key: lower disc (open symbols); upper disc (filled symbols).

that: (i) at a given flow-rate, when the other parameters are constant, mass transfer is higher at disc D_I than at disc D_S. This is due to the fact that D_I is impinged by the entering flow. However, the deviation between the results related to D_I and D_S decreases when h decreases (Fig. 4(a) and (b)) (i.e., when the mean radial velocity is increased, Q_v being constant), or when the entrance diameter $2R_1$ (Fig. 4(c)) (i.e., the size of the entrance impingement region) is decreased; and (ii) as h is reduced to a small value, the space between D_I and D_S tends to behave as a capillary, with a resulting increase in the pressure drop: the radial flow effect is made smaller, and the radial velocity profile is more uniform.

The double logarithmic plot of Fig. 5 shows, for disc D_I and $2R_1 = 14$ mm, the influence of h on the variation of $\overline{Sh}$ with Re. As h is increased, the slope of the straight lines obtained also increases but tends to stabilize: the Re exponent progressively changes from approximately 0.5 to 0.7. Furthermore, all the other parameters being constant, the hydrodynamics between the discs changes with h, and this explains the variation of $\overline{Sh}$ with Re. Indeed, in the absence of an impingement entrance region, it is evident (Fig. 6) that: (i) at small h values, the radial velocity profile can be uniform, parabolic or approximately parabolic, with a mean velocity which decreases with r. Hence, the hydrodynamic situation near D_I and D_S may be similar; and (ii) at high h values, the system tends to be similar to that in which a submerged jet impinges a solid surface; there is, therefore, a minimal influence of disc D_S on the flow structure, while a boundary layer flow takes place on disc D_I. For mass transfer to D_S the effect of Re is as $Re^{0.5}$ at small h values, but the Re exponent does not vary consistently when h is increased.

If Equation 1 did not apply, the dimensionless number X_2 could not be deduced and dimensional

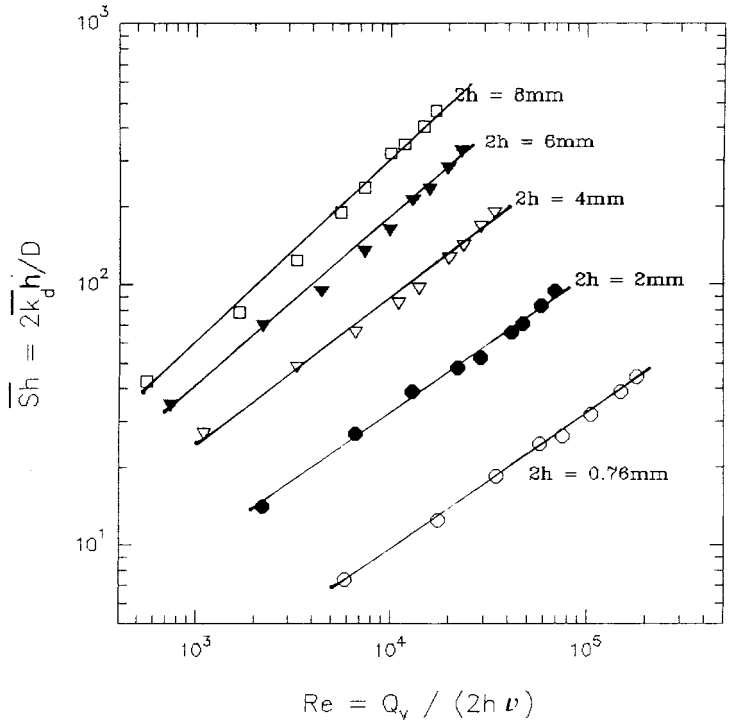

Fig. 5. Variation of $\overline{Sh}$ with Re for disc D_I. $2R_1 = 14$ mm. Key for $2h$: (□) 8, (▼) 6, (▽) 4, (●) 2 and (○) 0.76 mm.

analysis would be necessary. Such an analysis leads to the following empirical correlation:

$$\overline{Sh} = a\, Re^b\, Sc^c \left[\frac{h}{R_1}\right]^d \left[\frac{2h}{R_2 - R_1}\right]^e \qquad (11)$$

but, since the empirical determination of its exponents yields $e = 0.05$ and 0.08 for discs D_I and D_S, respectively, the influence of $2h/(R_2 - R_1)$ can be neglected. Finally, if $c = 1/3$, Equation 11 takes the form of the equation describing mass transfer between a planar solid surface and a liquid jet from a circular hole of diameter $2R_1$.

Another form of empirical correlation may be formulated:

$$\overline{Sh} = \text{constant} \times Sc^{1/3} \left\{\frac{2\,Re_m\, h^2}{R_2^2 - R_1^2}\right\}^{\alpha} \qquad (12)$$

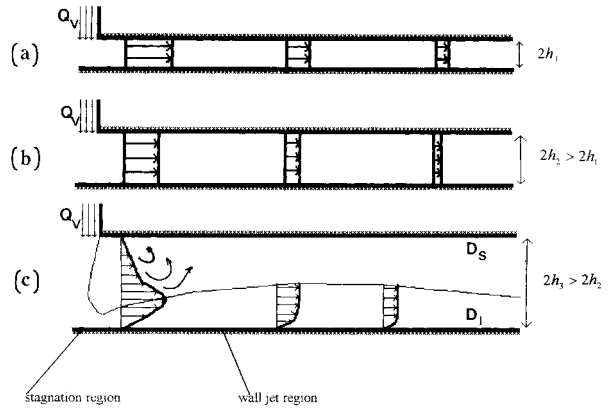

Fig. 6. Schematic evolution with $2h$ of radial flow between the discs.

that is, similarly to that used for the construction of Fig. 2(b). Representations of the data for discs D_I and D_S, respectively, were made in [19] accordingly to Equation 12. The empirical correlations obtained according to Equations 11 and 12 are given in Table 2. The Reynolds number exponent is not the same in the correlations related to disc D_I, while the weight given to h and to R_1 is approximately the same for a given disc, irrespective of the correlation.

4.2. *Local mass transfer*

The local measurements were restricted to $2R_1 = 6$ mm; $2h = 0.7$, 2 or 8 mm; $Q_v = 40\,dm^3\,h^{-1}$ for $2h = 2$ mm, that is, at $Re_m = 840$; $Q_v = 150\,dm^3\,h^{-1}$ for the three values of $2h$, that is, at $Re_m = 10000$; 3500 and 880, respectively. Figure 7(a), (b) and (c) shows, for three values of h, the distributions $k_d(r)$ obtained at $Q_v = 150\,dm^3\,h^{-1}$; Fig. 7(b) and (d) shows the influence of this parameter.

It can be observed that:

(i) Near $r = 0$, there exists on disc D_I a zone where k_d shows two maxima. In spite of the lack of precision, the radial position of the second maximum could delimit an entrance region of diameter $2R_1'$, different from $2R_1$. The values $R_1' = 6$, 9.5 and 13.5 mm indicate that the size of this region depends on h.

(ii) At $2h = 0.7$ and 2 mm, and outside the entrance region ($r \geq R_1'$), the experimental distributions $k_d(r)$ are practically identical. This finding confirms that the hydrodynamics are approximately the same near both discs when h is small, as anticipated from the discussion of Fig. 5.

Table 2. Empirical correlations obtained in the present work for discs D_I and D_S

Disc	*Correlation as Expression* 11	*Correlation as Expression* 12
Upper D_S	$\overline{Sh} = 0.36\,Re^{0.5}Sc^{1/3}\left(\frac{h}{R_1}\right)^{1.3}$ $(r = 0.97)$	$\overline{Sh} = 3.26\,Sc^{1/3}\left(\frac{2Re_m h^2}{R_2^2 - R_1^2}\right)^{0.5}$ $(r = 0.98)$
Lower D_I	$\overline{Sh} = 0.49\,Re^{0.5}Sc^{1/3}\left(\frac{h}{R_1}\right)^{1.44}$ $(r = 0.97)$	$\overline{Sh} = 2.76\,Sc^{1/3}\left(\frac{2Re_m h^2}{R_2^2 - R_1^2}\right)^{0.7}$ $(r = 0.98)$
Validity $550 \leq Re \leq 7 \times 10^4$ and $0.14 \leq h/R_1 \leq 0.8$		

(iii) When h is increased (Fig. 7(c)), the experimental distributions $k_d(r)$ are distinct, as anticipated in Fig. 6(c).
(iv) At $2h = 2$ mm, and in spite of the difficulty of interpreting a few points in Fig. 7(d), the two values of Re_m lead approximately to the same qualitative results.

Theoretical $k_d(r)$ distributions given by Equations 3 and 4, corresponding to laminar flow, are plotted in the four schemes of Fig. 7; they were calculated at positions between $r = R'_1$ and $r = R_2$ (external radius). It is clear that distribution (3) (parabolic profile) is in satisfactory agreement with the experimental data considering that the hydrodynamics are the same near both discs at radial distances higher than R'_1.

The mean mass transfer coefficients, computed from the measured overall limiting currents at the full cathodes D_I or D_S, may be compared to the corresponding mean values $[(\bar{k}_d)_I]_{int.}$ or $[(\bar{k}_{dS})]_{int.}$ resulting from the spatial integration of the experimental $k_d(r)$ distributions. It can be seen that the numerical values of the $[\bar{k}_d]_{meas.}/[\bar{k}_d]_{int.}$ ratio are near unity, except when the $k_d(r)$ distribution shows discontinuities which render the integration inaccurate; under such conditions, the ratio differs considerably from unity.

5. Discussion of the results

5.1. *Comparison with the literature*

5.1.1. Lower disc D_I. The results of Kreith [13] for air-to-solid mean mass transfer were used for comparison; in the experiments made in [13], the active region was essentially the domain $r \geq R_1$, while the impingement region $r < R_1$, where the mass transfer coefficient reaches high values [29], was made inactive. Figure 8(a) compares theoretical and empirical correlations from [13] with the current experimental results. The latter are somewhat higher, possibly because the impingement region over disc D_I was active in the authors' experiments. It is worth noting that the method used by Kreith (dissolution in air) is

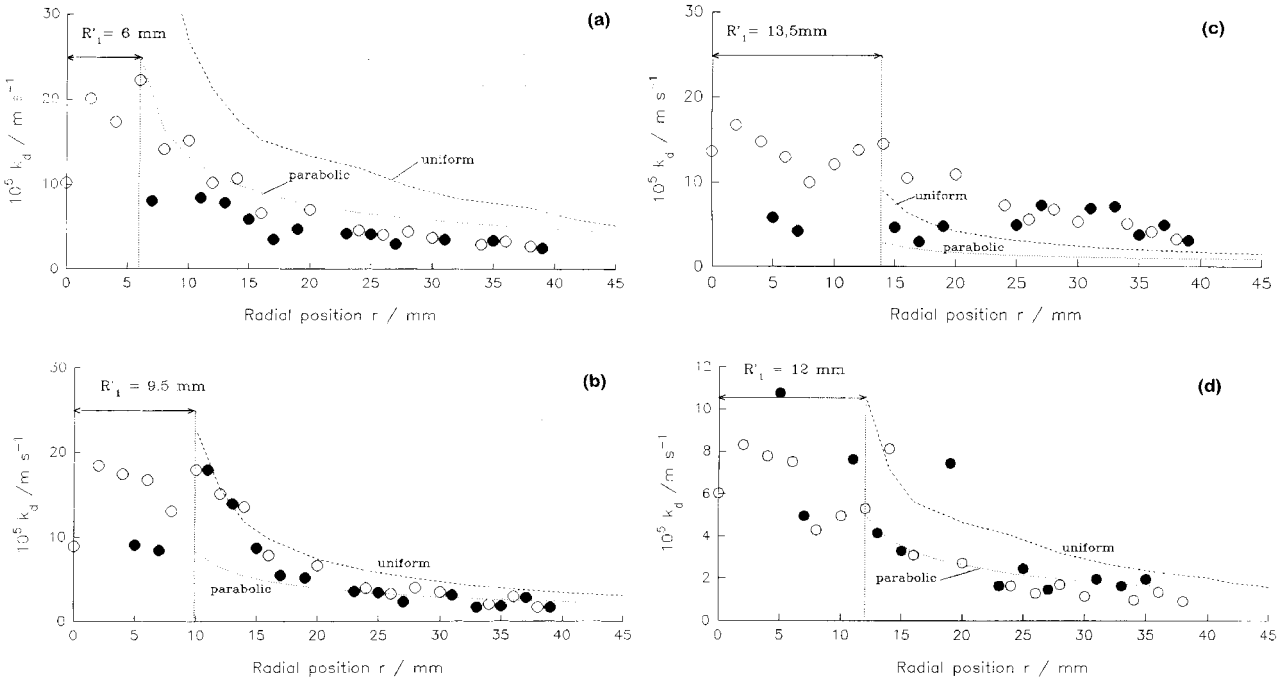

Fig. 7. Experimental $k_d(r)$ distributions. (a, b, c) at $Q_v = 150\,dm^3\,h^{-1}$ and three values of H; (d) at $Q_v = 40\,dm^3\,h^{-1}$ and $2h = 2$ mm. The ratio $(\bar{k}_d)_{meas.}/(\bar{k}_d)_{int.}$: (a) 1.03 (lower), 1.35 (upper); (b) 0.87 (lower), 1.10 (upper); (c) 0.97 (lower), 1 (upper); (d) 0.80 (lower), 0.89 (upper). Key: (○) lower disc, (●) upper disc.

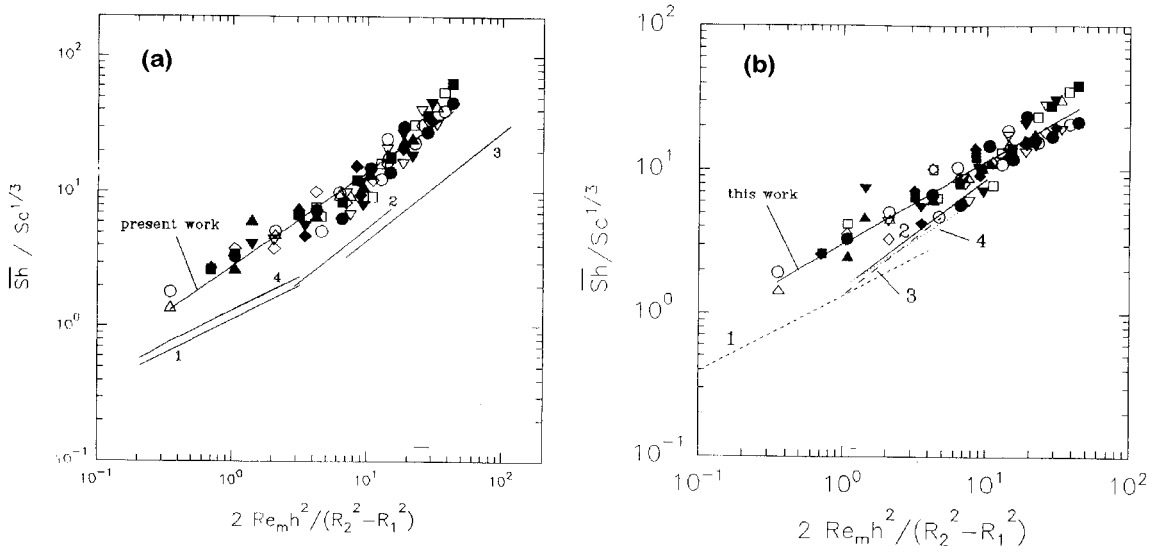

Fig. 8. Comparison of the present experimental results with correlations in the literature. Disc: (a) lower and (b) upper. Key for (a): (1, 2, 3) empirical results from Kreith *et al.* (see expressions T-1, T-2, T-3 in Table 1, respectively); (4) Theoretical (integrating Equation 4). Key for (b): (1, 2) Ashworth *et al.* [11]; (3) Ghoroghchian *et al.* [26]; (4) Jansson *et al.* [27].

probably less precise than the electrochemical method.

5.1.2. Upper disc D_S. To our knowledge, only the results of Jansson are relevant for comparison. The four corresponding correlations, given in Table 1, are compared in Fig. 8(b) to the current results. The agreement is satisfactory, in spite of a noticeable disagreement with one correlation arising from [11]. All the results shown in Fig. 8(b) were electrochemically obtained and corrrespond to wall-to-liquid mass transfer. The fact that in the work of Ghoroghchian *et al.* [26] $\bar{k}_d$ at disc D_S had a value which is intermediate between the cases of divergent and convergent flows (cell of Fig. 1(c)) is not discerned in Fig. 8(b).

5.2. *Discussion*

As demonstrated by local measurements, two different flow regions may be distinguished over disc D_I:

(i) The central region around the impingement point, which can be compared to the impingement region over a wall impinged by a jet in an unconfined system. A theoretical mass transfer study of the latter was made by Chin and Tsang [30]; following the nomenclature of the present work, the expression obtained by these authors may be written as

$$\overline{Sh} = 1.26\,Re^{0.5}\,Sc^{1/3}\,(h/R_1)^{1.44} \qquad (13)$$

(ii) The radial flow parallel to the disc region, with a mean velocity decreasing progressively with r. This can be compared to a region created by boundary layer flow over a flat plate or to the wall jet region below an impinging jet. In the former case, $\bar{k}_d$ would vary with $Re^{0.5}$ [31], while in the latter case $\bar{k}_d$ would vary with $Re^{0.75}$ [32]. Such considerations were also made by Bensmaili [33] in the analysis of mass transfer coefficients between a mercury surface and an impinging liquid jet. If comparison with only the boundary layer flow is considered, as a first approximation, integration between $r = R_1$ and $r = R_2$ of the local mass transfer expression established for the laminar boundary layer theory yields:

$$\overline{Sh} \approx 0.14\,Re^{1/2}\,Sc^{1/3}\left[\frac{2h}{R_2 - R_1}\right]\ln\left[\frac{R_2}{R_1}\right] \qquad (14)$$

Comparing Equations 13 and 14 to the authors' experimental data corresponding to $2R_1 = 14\,\text{mm}$ (Fig. 9), one may observe that: (i) at $2h = 8\,\text{mm}$, the results are located between results predicted by the boundary layer theory at low Re, and the solution corresponding to the stagnation point, towards which the results tend at high values of Re; and (ii) at $2h = 0.7\,\text{mm}$, a value for which the mean radial velocity in the channel is high, overall mass transfer is approximately the same for the two discs and is sufficiently well described by laminar boundary layer theory. However, the mass transfer is somewhat higher at disc D_I than at disc D_S. Fig. 7(a) indicates agreement between the theoretical distribution obtained by Kreith in the case of a laminar flow with a parabolic velocity profile and local mass transfer data.

Acknowledgements

E. Bezerra Cavalcanti acknowledges receipt of financial support from the CNPq of Brazil. The authors would like to thank Prof. Legrand and colleagues (Saint Nazaire, France) for making possible the experimental determinations of local mass transfer coefficients in their laboratory. The authors are grateful to Prof. T. Z. Fahidy (University of

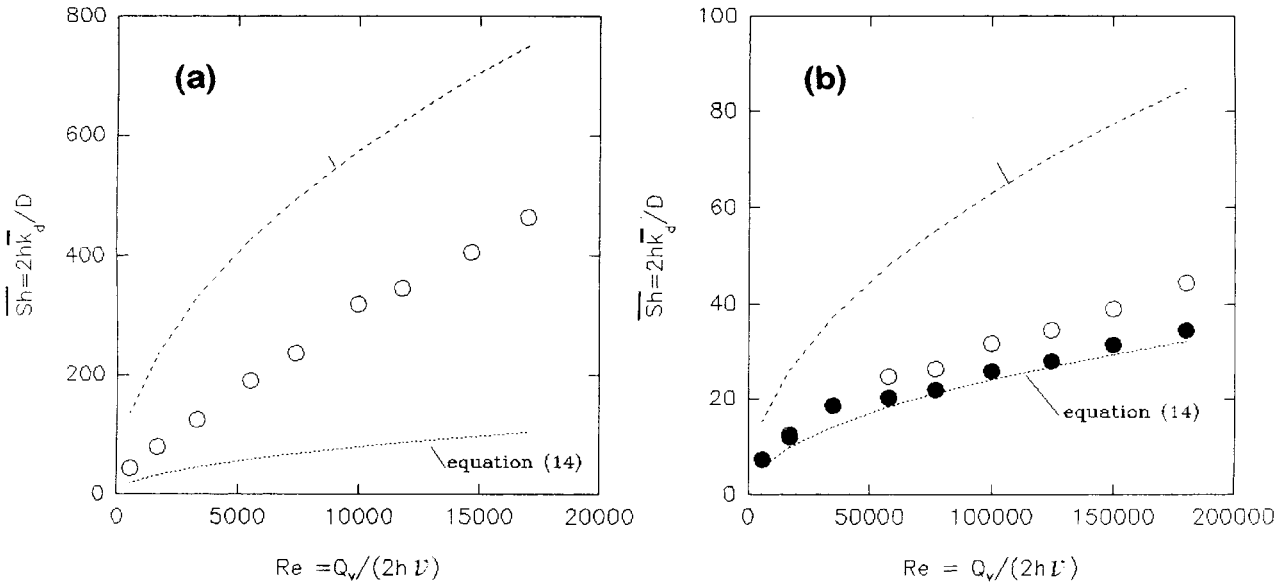

Fig. 9. Sherwood number as a function of the Reynolds number. (a) Lower disc, D_I, $2h = 8$ mm; (b) upper disc, D_S, $2h = 0.7$ mm. Key: (- - - -) Equation 13; (·····) Equation 14; (●) upper disc; (○) lower disc.

Waterloo, Canada) for his valued help in improving the English language of the paper.

References

[1] P. S Moller, *The Aeronautical Quartely* (May 1961) 183.
[2] J. L. Peube, J. Méc. (France) **4** (1963) 377.
[3] S. B. Savage, *J. Appl. Mech.* (Dec. 1964) 594.
[4] C. P. Chen and J. L. Peube, *C.R. Acad. Sci. Paris* **258** (1964) 5353.
[5] E. Bakke, J. F. Kreider and F. Kreith, *J. Fluid Mech.* **5** (1973) 209.
[6] J. D. Raal, *ibid.* **85** (1978) 401.
[7] C. R. Truman and D. F. Jankowski, *Int. J. Heat Fluid Flow* **6** (1985) 69.
[8] F. B. Thomas, P. A. Ramachandran, M. P. Dudukovic and E. E. W. Jansson, *J. Appl. Electrochem.* **18** (1988) 768.
[9] R. K. Horn, *AIChE J.* **75** (1979) 125.
[10] F. Wenisch, H. Nobe, H. Hannebaum, R. K. Horn, M. Stroezel and D. Degner, *ibid.* **75** (1979) 14.
[11] G. A. Ashworth and R. E. Jansson, *Electrochim. Acta* **22** (1977) 1295.
[12] R. V. Shenoy and J. M. Fenon, *Int. J. Heat Mass Transfer* **33** (1990) 2059.
[13] F. Kreith, J. H. Taylor and J. P. Chong, *J. Heat Transfer* (May 1959) 95.
[14] G. M. Brown, *AIChE J.* **6** (1960) 179.
[15] F. Kreith, *Int. J. Heat Mass Transfer* **9** (1965) 265.
[16] F. Kreith, 'Transfert de Chaleur et de Masse dans un Ecoulement Radial Entre Deux Disques Parallèles Fixes, ou Tournant à la même Vitesse', Thesis, University of Paris, France (1965).
[17] F. Kreith, *C. R. Acad. Sci. Paris* **260** (1965) 62.
[18] S. Sarveswara Rao, C. V. S. K. Prasad and G. J. V. J. Raju, *Indian J. Technol.* **23** (1985) 47.
[19] E. B. Cavalcanti, 'Transfert de Matière aux Electrodes d'une Cellule Combinant Ecoulement Forcé et Rotation', Thesis, University of Rennes 1, Rennes, France (1997).
[20] E. B. Cavalcanti and F. Coeuret, *J. Appl. Electrochem.* **26** (1996) 655.
[21] A. Bensmaili, 'Etude du Transfert de Matière Associé à l'Impact de Jets Liquides Simples ou Multiples sur des Surfaces Solides ou Liquides', Thesis, University of Rennes 1, France (1991).
[22] A. Bensmaili and F. Coeuret, *Int. J. Heat Mass Transfer* **33** (1990) 2743.
[23] G. H. Vatistas, *AIAA J. (USA)* **28** (1989) 1308.
[24] R. A Thomas and M. H. Cobble, *Trans. ASME, Ser.C*, **5** (1963) 189.
[25] D. J Pickett, 'Electrochemical Reactor Design', (Elsevier, Oxford, 1979), p. 138.
[26] J. Ghoroghchian, R. E. W. Jansson and R. J. Marshall, *Electrochim. Acta* **24** (1979) 1175.
[27] R. E. W. Jansson and R. J. Marshall, *J. Appl. Electrochem.* **8** (1978) 287.
[28] J. R. Selman, Mass Transfer Measurements by the Limiting Current Technique, *in Adv. Chem. Eng.* (Academic Press, New York), **10** (1978) 212.
[29] F. Coeuret, *Chem. Eng. Sci.* **30** (1975) 1257.
[30] D. T. Chin and C. H. Tsang, *J. Electrochem. Soc.* **125** (1978) 1461.
[31] V. G. Levich, 'Physicochemical Hydrodynamics', (Prentice Hall, Englewood Cliffs, NJ, 1962), p. 87.
[32] M. B. Glauert, *J. Fluid Mech.* **1** (1956) 625.
[33] J. Yamada and H. Matsuda, *Electroanal. Chem. Interf. Electrochem.* **44** (1973) 189.
[34] A. Bensmaili and F. Coeuret, *Can. J. Chem. Eng.* **73** (1995) 85.